STUDY ON PHENOTYPIC CHARACTERISTICS OF MILLET BASED ON 3D MODEL
/
基于三维模型的谷子表型特征分析研究

Lili SUN [1], Yaoyu LI [2)], Yuzhi WANG [2)], Weijie SHI[2)], Wuping ZHANG [2)], Xiaoying ZHANG [3)], Huamin ZHAO [1)], Fuzhong LI [2,*)]

[1)] College of Agricultural Engineering, Shanxi Agricultural University, Taigu, Shanxi / China
[2)] College of Software, Shanxi Agricultural University, Taigu, Shanxi / China
[3)] Department of Basic, Shanxi Agricultural University, Taigu, Shanxi / China
Tel: +8603546287093; E-mail: lifuzhong@sxau.edu.cn
Corresponding author: Li Fuzhong
DOI: https://doi.org/10.35633/inmateh-69-55

Keywords: *Millet phenotype, Camera calibration, 3D reconstruction, Point cloud filtering, Character extraction*

ABSTRACT

As one of the ancient cultivated crops in China, millet has the characteristics of high nutritional value, drought resistance and barrenness. It also plays an important role in ensuring the supply of food in our country. At present, most of the millet breeding work uses manual extraction of phenotypic information, which is labor-intensive and inefficient. Therefore, the development of an automated, efficient and accurate millet phenotype detection method has practical significance for the extraction of the millet genome. In this study, a combination of sparse reconstruction based on Structure from Motion (SfM) and Patch-based Multi-View Stereo (PMVS) was used to select three different varieties of millet. A total of 81 samples of 9 samples in each period were reconstructed to obtain a 3D model of millet. The combination of conditional filtering and statistical filtering is used to remove the noise points generated during the photographing process, and finally the obtained point cloud data is used to measure the agronomic traits of millet such as plant height and leaf area. The results show that the interval angle of 5° is the best reconstruction angle of millet. The coefficient of determination R^2 of point cloud measurement results and manual measurement data regression analysis is higher than 0.94, indicating that the method used for 3D reconstruction has high applicability to different millet in different periods and high-throughput measurement of millet by the method in this paper is feasible. This study provides a theoretical basis for a millet phenotypic information measurement device.

摘要

谷子作为中国古老的栽培作物之一，具有营养价值高、抗旱耐贫瘠等特点。对我国粮食的供给保障也具有重要作用。目前，谷子育种工作多采用手工提取表型信息，劳动量大，效率低下，所以发展一种自动化、高效且精确的谷子表型检测方法对于谷子基因组的提取具有实际意义。本研究采用了基于运动恢复结构（SfM Structure from Motion）的稀疏重建和基于面片的多视角立体几何（PMVS Patch-based Multi-View Stereo）相结合的方法，对三个不同品种的谷子选取三个不同时期每个时期 9 个样本，共 81 个样本进行三维重建得到谷子的三维模型。利用条件滤波和统计滤波相结合去除在拍照过程中产生的噪声点，最后利用得到的点云数据对谷子进行株高、叶面积等农艺性状的测量。结果表明隔角度为 5° 为谷子的最佳重建角度。点云测量结果与人工测量数据回归分析决定系数R^2均高于 0.94，表明采用的方法进行三维重建对于不同时期不同谷子有较高的适用性并且通过本文的方法对谷子进行高通量测量是切实可行的。本研究为谷子表型信息测量设备提供了理论基础。

INTRODUCTION

China has the largest millet cultivation area and the largest yield in the world. The sown area accounts for more than 90% of the world's sown area. Millet belongs to the Gramineae setaria, with strong drought

[1]*Lili SUN, Ph.D. Eng.; Yaoyu LI, M.S. Stud. Eng.; Yuzhi WANG, M.S. Stud. Eng.; Weijie SHI, M.S. Eng.; Wuping ZHANG, Prof. Ph.D. Eng.; Xiaoying ZHANG, Prof. Ph.D. Eng.; Huamin ZHAO, Ph.D. Eng. ; Fuzhong LI, Prof. Ph.D. Eng..*

resistance and desert resistance, being the ideal crop of dry farming, in Inner Mongolia, Shaanxi, Shanxi and other areas of arid agricultural areas widely planted.

Recently, computer vision has been widely used in crop phenotypic research. The commonly used method is through the image processing technology from crops two-dimensional or three-dimensional images to extract the relevant properties parameters, production forecast and related analysis, etc. 3D models of crops contain spatial information that two-dimensional images do not have, from which more comprehensive and more real phenotypic parameters can be extracted, such as leaf area, plant type, photosynthesis related parameters, etc. (*Gao T. et al., 2021, Xu B. et al., 2017, Rupnik E. et al., 2018, Collier S. et al., 2017*.)

In recent years, more and more people are combining computer vision technology with agriculture to help breeders analyze and screen crop varieties for salt tolerance, drought tolerance and disease resistance. Automatic extraction of sorghum morphological characteristics was realized by 3D point cloud data analysis (*Xiang L, et al., 2019*). *Fang Wei et al. (2016)* proposed a fast 3D reconstruction method for obtaining traits of high-throughput plant types. *Qiu Q. et al. (2019)* used 3D LiDAR point cloud to conduct high-throughput phenotypic analysis on maize plants in the field. *Hu (2018)* calculated crop plant height in the field with UAV high throughput. He used Kinect V2 to obtain color images and depth images of citrus trees, and removed the background by depth threshold segmentation method, and carried out real-time 3D reconstruction of orange tree crowns, which was used for citrus picking barriers. *Syngelaki M. et al., (2018),* designed Photogrammetry system. This system constructed a stereo photogrammetry system consisting of a digital single-lens reflex camera, a lighting platform for placing petri dishes and an Arduino board to control the image acquisition process. The camera was mounted on a bracket. The camera can rotate at 30°, 45° and 60°, so as to obtain multi-view sequence images in different directions. Then Opencv and PCL technologies are used to conduct THREE-DIMENSIONAL reconstruction of biological samples in petri dishes. *He et al. (2017)* built a low-cost multi-view stereo imaging system, which can collect image data of Strawberry Fruit 360. Grass was constructed based on SFM and MVS technology. *Wen et al. (2021)* proposes a 3D phytomer-based geometric modelling method with maize (Zea Mays) as the representative plant. Specifically, conversion methods between skeleton and mesh models of 3D phytomer are specified. *Schipper et al. (2023)* calibrated and validated an existing functional structural plant model (FSPM), which combines plant morphology with a ray tracing model to estimate light absorption at leaflet level."

MATERIALS AND METHODS

Experimental materials

Three representative millet varieties, namely Jingu 21, Dabaigu, and Yuanping Xiaogu, were selected as experimental materials. Under the same temperature, humidity and light conditions, 30 plants were selected from each variety, and 10 plants were selected from jointing stage, heading stage and filling stage respectively for measurement.

Imaging system mainly includes a visible light camera (Cannon EOS 1300D), Hong Xing Yang electric rotating platform, 4 pieces of the LED face plate, a programmable logic controller and computer system objects are shown in Fig. 1. A fixed camera on a tripod, height and back angle of depression all can be adjusted according to actual condition. Rotating platform can be rotation angle according to need and time interval set.

Fig. 1 – Imaging system

In this paper, Zhang Zhengyou calibration method (*Zhou, et al., 2009*) was used to obtain the internal and external parameters and distortion coefficient of the camera to correct the camera. The plants were placed on the rotating platform, and the camera was used to take photos of millet. Different intervals were selected at 1°, 2°, 3°, 5°, 10° and 15°, respectively, and six groups of millet photos with different sequences were obtained. When taking photos, the distance between the camera and the position between the plants should be kept within 25 cm, and all the leaves of the plant should be in the field of view of the camera. Rotate once each time, and take photos when all the leaves of the plant do not shake.

3D reconstruction method

In image-based 3D reconstruction of crops, images are acquired by camera, then sparse reconstruction based on motion recovery structure is carried out, and then the reconstructed sparse point cloud is reconstructed based on faceted multi-view stereo geometry. Finally, point cloud filtering is carried out to obtain clear 3D point cloud image.

The main algorithm principle is as follows:

Sparse reconstruction based on SfM

Feature detection and matching: it is the first step of 3D reconstruction to efficiently and accurately detect and match feature points in the image. The feature points of the image are composed of key points and descriptors. Key points are feature points with image location information, some of which also have direction and scale information. Descriptors are used to describe the information of pixels around key points. Generally speaking, the design principle of descriptors is that similar descriptors should be designed according to similar features in appearance. Therefore, when matching, two feature points can be regarded as the same feature points as long as their descriptors are close in the vector space (*Steve H. et al., 2015*).

The detection and matching steps of feature points are as follows: firstly, extract the pixel of feature in the image. The scale-invariant feature transform (SIFT) algorithm was adopted to construct scale space by differential Gaussian convolution of images at different scales (*Lowe D., 2004*). Non-maximum suppression was used to determine the feature points, remove the low contrast points, and then remove the edge points by Hessian matrix, and then determine the main direction of the feature points. Finally, descriptors of feature points are calculated according to the key points obtained. In order to keep the invariance of scale, when calculating the descriptors of feature points, the image is usually transformed to a unified scale space and scale factors are added. Similar to scale invariance, in order to maintain rotation invariance, the direction information of key points is added to the calculation of feature point descriptors. Finally, the matching is carried out according to the descriptors of feature points.

Basic matrix estimation

There are polar geometric constraints for the same point in different images (*Qi Z. et al., 2018*). Antipolar geometry is the internal projective geometry between two views, independent of landscape structure and dependent only on the internal and external parameters of the camera. Essentially, the antipolar geometry between two views is the geometry of the intersection between the image plane and the plane bundle whose axis is the baseline (the line connecting the centers of the two cameras).

As a mathematical expression of the polar geometry constraint, the basic matrix only depends on the internal and external parameters of the camera, and the specific expression is as follows:

$$F = K^T t \times RK^{-1} \quad (1)$$

where:

K represents the internal parameter of the camera, R and T represent rotation and translation of the camera.

Essential matrix estimation

The intrinsic matrix is obtained by removing the camera's internal parameters from the basic matrix. Its purpose is to constrain the matching obtained before, and the matching obtained becomes geometric consistent matching. The specific expression of the intrinsic matrix is as follows:

$$E = t \times R \quad (2)$$

Three-dimensional point cloud computing

Using the known coordinates of the matching points and the internal and external parameters of the camera, the 3D coordinates of the matching points are restored. Through iterative calculation, new images are constantly added, and the sparse point cloud of millet is finally obtained.

PMVS Patch-based Multi-view Stereo (MVS)

Since sparse point cloud contains less information, dense reconstruction is needed to obtain the dense point cloud of millet. The basic idea of MVS is to find the point of image consistency among different images in an image sequence. MVS can be divided into three categories (*Seitz S., 2006*): dense reconstruction based on voxel, the rest on another, and dense reconstruction based on fusion of dense depth map reconstruction, including the rest based on another dense reconstruction does not require any initial information, such as initial bounding box or initial parallax scope, its applicable scope is very broad, so this paper selected based on the dense reconstruction.

As shown in Fig. 2 in the dense reconstruction based on the plane, the plane P is determined by its center $C(p)$ and the unit normal vector $N(p)$ pointing to the camera shooting it. A reference image $R(p)$ is associated with each facet P, and $R(p)$ selects the image that is nearly parallel to the facet P, which has the smallest distortion. Conversely, the reference plane determines the orientation and scope of the rectangle, perpendicular to $n(p)$, so that the projection of one of its edges in $R(p)$ is parallel to the image pixel row, and its corresponding minimum area in $R(p)$ is $\mu \times \mu$. One is $S(p)$, which means P is visible in the image, but there is an image that is not easy to be recognized or blocked by objects. $T(p)$ represents the image where P is really seen, and $R(p)$ is naturally contained in $S(P)$. Two strong constraints are added to the plane model. First, the constraint of local width consistency is added to require the projection texture of each plane P to be continuous on at least γ images. Second, to add global visual consistency, it is required that the surfaces do not block each other in $S(p)$.

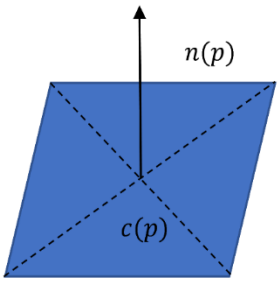

Fig. 2 – Sketch map

Each image I was associated with a regular cell $C(I,J)$, whose size was $\beta_i \times \beta_i$ pixels, trying to correspond to a facet for each cell, as shown in Fig. 3 Cell $C\ (I,j)$ tracks two different sets of reconstructed facet sets $Q_I(i,j)$ and $Q_f(i,j)$, among which two facet sets may be visible in $C(i,j)$: if $I \in T(p)$, another is stored in the $Q_I(i,j)$, if $I \in S(p)/T(p)$, is stored in the $Q_f(i,j)$. At the same time, associate the surface center of $C(i,j)$ and $Q_f(i,j)$ with the center depth of the camera nearest to it, which is equivalent to assigning a depth map to each image I, which will be used in the subsequent visual calculation.

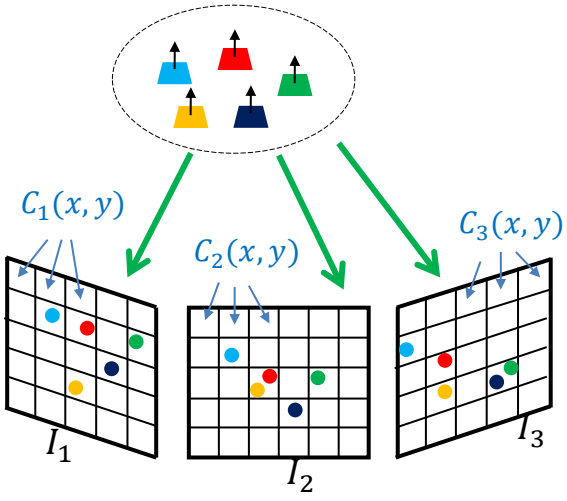

Fig. 3 – Image and cell diagram

Given a surface p, its projection normalized correlation function (NCC) $N\ (p, I, J)$ on two images I and J is used to measure their gray consistency. Given a surface p, its reference image is $R(p)$, and the image set $T(p)$ of truly visible p can be calculated by maximizing its average NCC value to find the position $C(p)$ of the surface and its normal vector $n(p)$.

$$\bar{N}(p) = \frac{1}{|T(p)|-1}\sum_{I\in T(p),I\notin R(p)} N(p,R(p),I) \quad (3)$$

In order to simplify the calculation, $c(p)$ is appointed to simplify the worthiest problem into three dimensions on the ray composed of the optical center of the reference camera and the corresponding image points, that is, to obtain the depth and the yaw Angle and pitch Angle of the normal vector $n(p)$ on the ray, and then obtain the group optimization parameters by using the conjugate gradient method. In the actual calculation, a simple method is used to obtain initial estimates of $c(p)$ and $n(p)$.

The above process is based on the assumption that the surface of the scene or object is a diffuse reflection surface, but when the object or scene reflection surface is specular reflection or there are obstacles, the above method cannot obtain the ideal effect. The influence of the non-diffuse plane can be reduced by ignoring the images with smaller normalized cross-correlation mean value. That is, a threshold α is set in advance, and the image will be adopted only when the luminosity difference between the image and its reference image $R(p)$ is less than the threshold α.

$$N^*(p,R(p),I) = \{I|I \in T(p), N(p,R(p),I) \le \alpha\} \quad (4)$$

$$\bar{N}(p) = \frac{1}{|T(p)|-1}\sum_{I\in T(p),I\notin R(p)} N^*(p,R(p),I) \quad (5)$$

By limiting the brightness difference value, the algorithm effectively avoids the occurrence of non-diffuse reflection or obstacles in the image $R(p)$.

The visibility of each facet is determined by the set of images $S(p)$ and $T(p)$ from which it can be seen (partially or truly visible). In the process of dense reconstruction, two slightly different methods are used to reconstruct $S(p)$ and $T(p)$ respectively. After the matching stage is completed, the surface is reconstructed by matching features, and the visibility of the surface must be determined by the consistency of gray level. Specifically, the image whose NCC value of the connected image set exceeds a certain threshold value is initialized.

$$S(p) = T(p) = \{I|N(p,R(p),I) > \alpha_0\} \quad (6)$$

On the other hand, in the diffusion process, the surfaces are associated with the depth of the left and right images after sufficiently dense reconstruction, and for each surface, $S(p)$ is obtained by specifying a threshold value for its depth. That is: $S(p) = \{I|d_I(p) \le d_I(i,j) + \rho_1\}$. Where $d(p)$ is the ray depth of P on corresponding image I, $d_I(i,j)$ is the depth in cell $C(i,j)$ related to image I and plane p, and ρ_1 is the distance at depth $C(p)$ after the displacement β_1 of corresponding image $R(p)$. Once S(p) is estimated, gray consistency is used to determine where the plane P is actually seen.

Through $T(p) = \{I \in S(p)|N(p,R(p),I) > \alpha_1\}$ is Confirmed, this method requires the reference image $R(p)$ to be the real p, otherwise this method will fail. In order to avoid this situation, relevant methods to deal with this problem will be introduced later in this paper. The reliability and consistency of visual information can also be improved by iterative matching and filtering.

PMVS algorithm needs to establish at least one facet for each image cell $C(i,j)$, and this process mainly has three steps:

✓ Firstly, feature matching. The motion recovery structure algorithm can obtain the sparse point cloud structure and camera parameters of the scene. Therefore, the output of the motion recovery structure algorithm is used as the input in this study to complete the process of initialization of sparse surface slices without feature extraction and matching. According to the sparse point cloud information, the root node of the octree can be initialized, that is, a cube that just completely covers the sparse point cloud.

✓ Secondly, surface diffusion, in which a sparse set of surfaces is obtained from a dense set of surfaces, that is, new surfaces are added around existing surfaces by iterative method until they cover the entire surface of the object or scene. More intuitively, given two faces p and p', if they are stored in adjacent cells $C(i,j)$ and $C'(i,j)$ of the same image I, and their tangent planes are adjacent, the two faces are said to be adjacent and only new adjacent faces are created where diffusion is necessary, i.e., the face set $Q_i(i',j')$ is empty, and there are no elements in $Q_f(i',j')$ and p is n adjacent relation, where the n nearest neighbor relation of p and p' is:

$$|(c(p)-c(p'))\cdot n(p)|+|(c(p)-c(p'))\cdot n(p')|<2\rho_2 \quad (7)$$

The calculation method for ρ_1 is the same as that for ρ_2, which is the corresponding distance where the midpoint of $c(p)$ and $c(p')$is depth after $R(p)$ shift β_1 of the corresponding image.

✓ Thirdly, surface filtering: The purpose of filtering is to remove the surfaces inside and outside the scene or object surface and get an accurate dense point cloud model. Filtering has two steps, further implementing the principle of viewpoint consistency in the front diffused and reconstructed surfaces and removing false matching the first filter is to remove the surfaces outside the real scene or object surface. Suppose there is a sheet p_0, belonging to the set of sheets U containing it. Remove sheet p_0 if sheet p_0 satisfies the following equation. More intuitively, if sheet p_0 is an external value, then the value of $N(p_0)$ and $T(p_0)$ should be small and p_0 is more likely to be removed. The second filter is to remove objects in the scene or real internal surface, using the image depth map, related recalculate the rest for each another $S(p_0)$ and $T(p_0)$, when $|T(p_0)|<\gamma$, remove p_0. Notice that the way you compute $S(p_0)$ and $T(p_0)$ is different from the way you get them in the diffusion process, because after the reconstruction of p_0, more p_0 has been reconstructed.

Finally perform a weak regularization process: p, rest for each another statistical image set $S(p)$ contains its cells and facets in surrounding cells, cell and around for n and p in rest if a group of another neighbor is less than the proportion of the $\varepsilon=0.25$, p was removed as a value outside the threshold of α_1 initial value is 0.7, the diffusion and filtering iterative steps after the completion of the threshold value of α_1 set the value of 1.

$$|T(p_0)|\bar{N}(p_0)<\sum_{p_j\in U}\bar{N}(p_j) \quad (8)$$

The dense point cloud of millet was obtained by using PMVS algorithm for sparse point cloud structure obtained by SfM and internal and external parameters of camera.

Conditional filter and statistical filter remove noise points

There are a large number of noise points in Formula 8. Only by removing noise points, outliers and holes in filtering pretreatment, can the subsequent steps such as registration, feature extraction and surface reconstruction be better carried out. In this paper, conditional filtering and statistical filtering are used to remove noise points.

RESULTS AND DISCUSSION

Influence of interval angle on point cloud precision

The data sets of the images of the three millet varieties in the same growth cycle were named as Dabaigu_ n, Jingu 21_ n and Yuanping Xiaogu_ n according to different rotation interval angles (n=1,2,3,5,10,15) and n is the interval angle between two adjacent pictures of the dataset. By 3D reconstruction of 18 datasets, the effects of different varieties on the reconstruction accuracy at different intervals were tested.

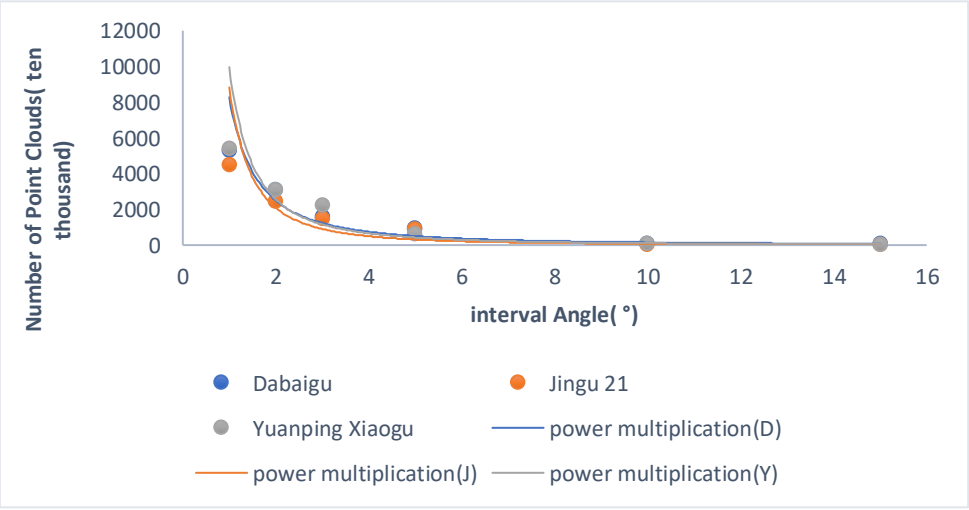

Fig. 4 - Number of point clouds for different varieties of millet at different intervals

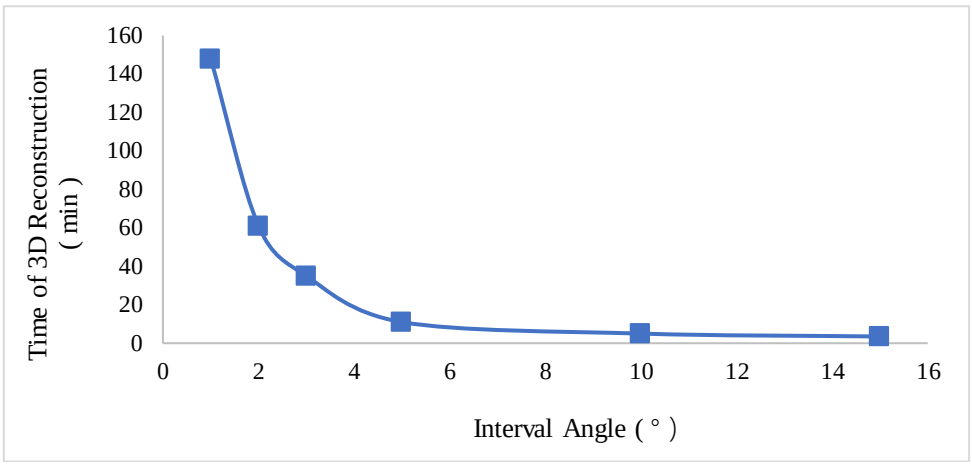

Fig. 5 - Time of 3D reconstruction of millet at different intervals

It can be seen from Fig.5 that the smaller the interval angle, the more reconstructed views, the more points of the reconstructed result cloud, and the closer the reconstructed result is to the reality. According to Figures 5 and 6, when the interval angle is less than 5, the number of point clouds keeps increasing, but the running time of the program will increase significantly. Therefore, considering the processing time and point cloud precision comprehensively, interval angle 5 is the best reconstruction interval angle.

Measurement of millet phenotype

In this paper, 3D reconstruction was carried out for the three varieties at jointing stage, heading stage and filling stage, and 9 plants were selected in each stage and 81 plants in total were photographed for reconstruction. Each plant was photographed at an interval Angle of 5. A total of 72 photos were taken to obtain three-dimensional point cloud reconstruction, and the obtained point cloud data were used to calculate the plant height, leaf area and other agronomic traits of the samples.

Phenotype measurement method

The phenotypic traits measured in this paper were defined as follows: Plant height is from the highest point of the plant to the edge of the planting pot. The leaf area is the sum of leaf areas of all point clouds on each leaf of millet. 3D reconstruction of three varieties of millet was carried out to obtain the corresponding point cloud data, and the point cloud data was used to measure the phenotype of millet. The 3D measured area and manual measured area (real area) as well as the 3D measured plant height and real plant height of the three varieties of millet were regression, as shown in Fig. 5. It can be seen from the figure that the coefficient $R2$ between the measured leaf cumulus cloud area and the artificial real measured area of Dabaigu, Yuanping Xiaogu and Jingu 21 are 0.94, 0.94 and 0.94 respectively; The coefficient $R2$ between the measured cloud height and the measured artificial height were 0.97, 0.97 and 0.96; The correlation between them was tested and the results showed that the correlation was significantly different at the level of 0.05. It is proved that the high throughput measurement of plant height and leaf area by three-dimensional model has high accuracy.

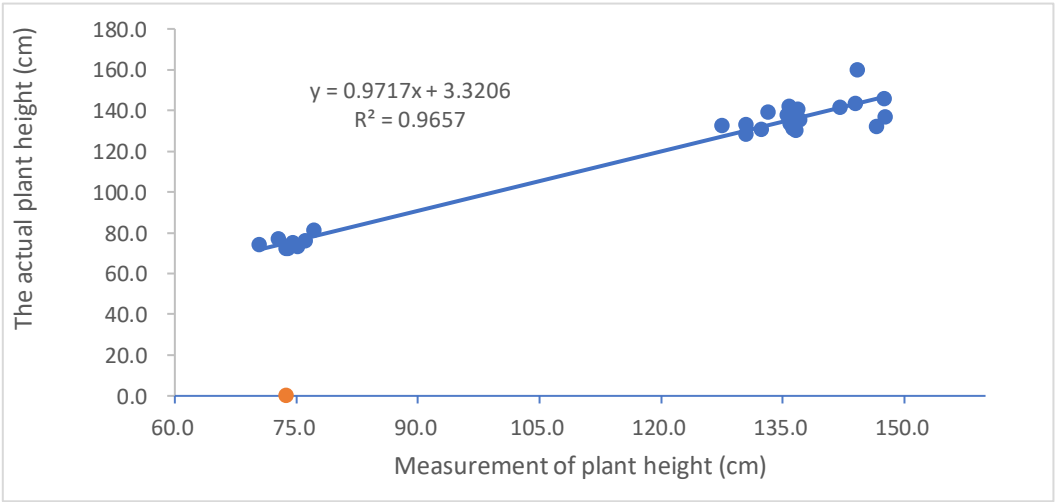

a)

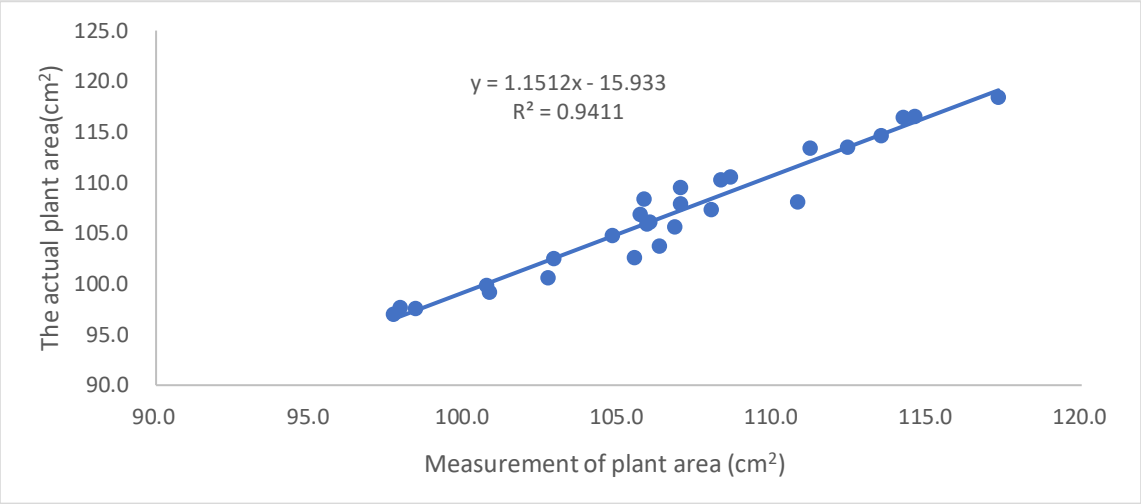

b)

Fig. 6 - Comparison of 3D measurement data of Jingu 21 with real data

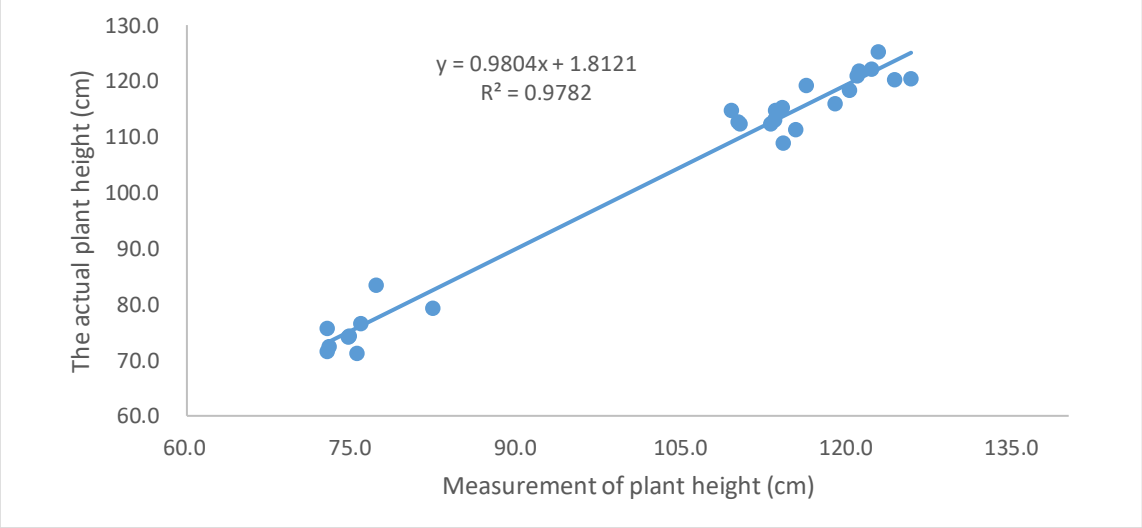

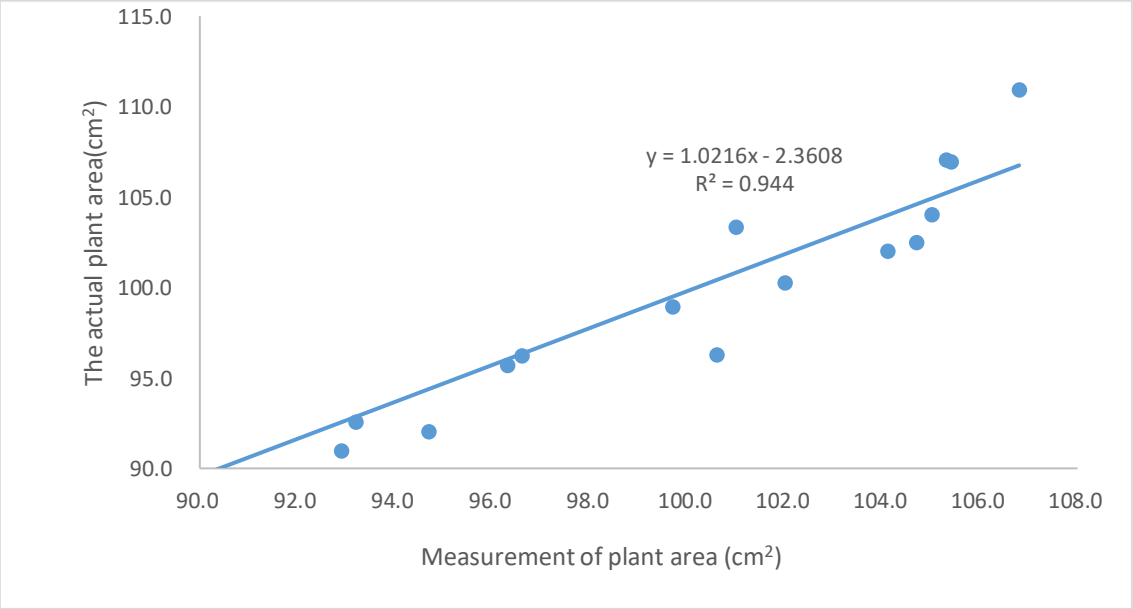

Fig. 7 - Comparison of 3D measurement data of Yuanping Xiaogu with real data

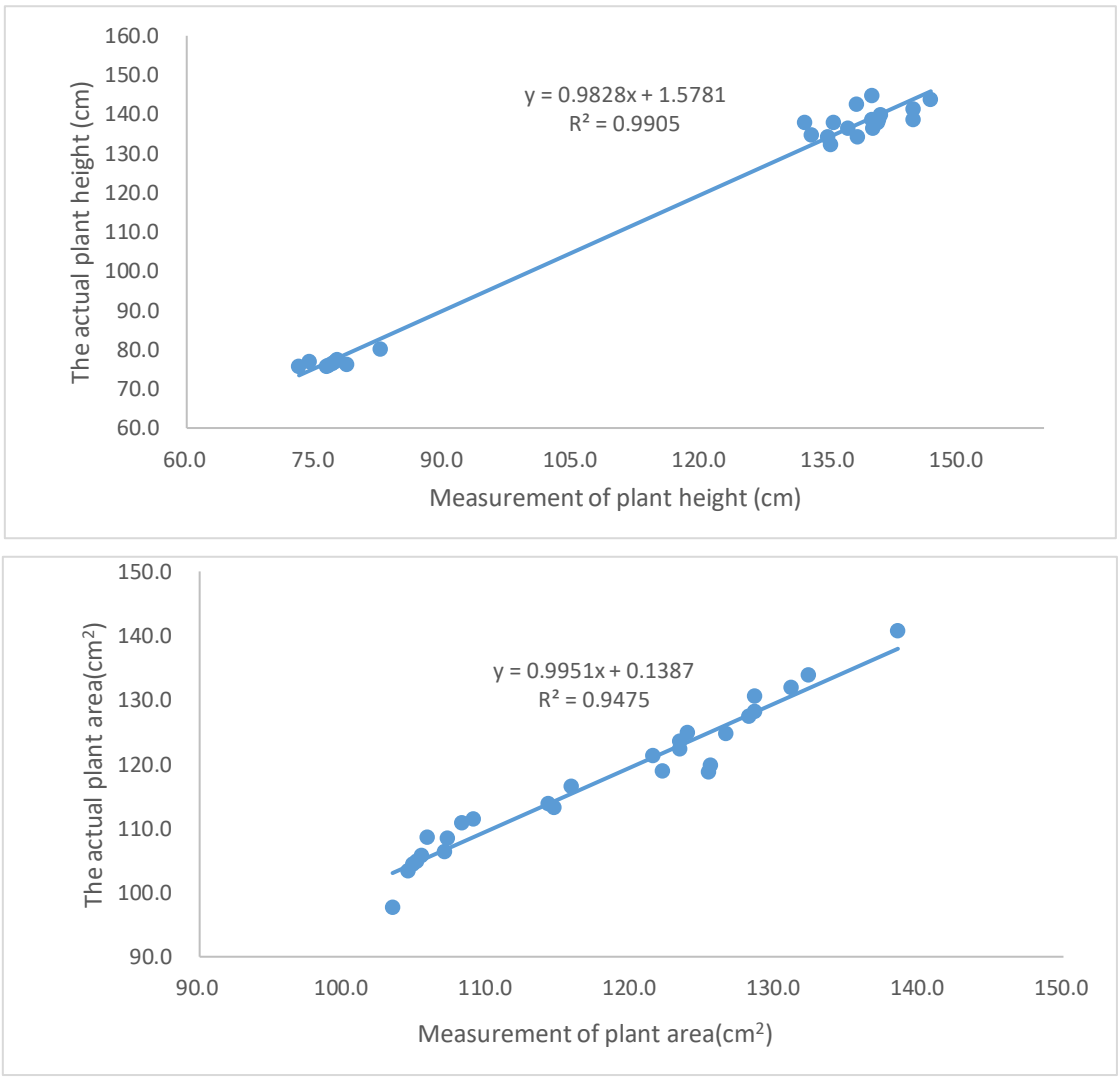

Fig. 8 - Comparison of 3D measurement data of Dabaigu with real data

Table 1

Analysis of phenotypic differences between varieties

Variety	Leaf area (cm2)	Plant height (cm)
Dabaigu	113.87 a	123.30 a
Yuanping Xiaogu	103.69 b	104.58 b
Jingu21	92.33 c	100.20 b

Note: Different lowercase letters in the same column indicate a significant difference of P<0.05.

As can be seen from Table 1, at the significant level of 0.05, the difference in leaf area among the three varieties was caused by the difference among varieties, and the difference in plant height among Dabaigu, Yuanping Xiaogu and Jingu 21 was caused by the difference among varieties.

CONCLUSIONS

This paper studies a method to reconstruct three-dimensional point cloud of millet by image sequence. The method uses SfM and PMVS to carry out 3D reconstruction of millet, and uses conditional filtering and statistical filtering to filter the point cloud of millet. Through the comparison of the reconstruction accuracy and speed of the shooting data set of 3 different millet varieties with different interval angles, it was concluded that when the shooting interval was 5, the reconstruction accuracy of millet met the experimental requirements and the time was faster. Then, the 3D point cloud data of millet was used to analyze the plant height of millet, nondestructive measurement of leaf area, and regression analysis and manual analysis of the measured data.

When the spacing Angle was 5, the determining coefficients of plant height and leaf area of three kinds of millet were higher. In conclusion, the method adopted in this paper has high applicability to millet samples of different varieties and different periods, and provides a reliable basis for the analysis of 3D phenotypic traits of millet. However, the parameters measured in the study are still few, and further research is needed on how to obtain the number of leaves and canopy structure of millet from point cloud data.

ACKNOWLEDGEMENT

The authors were funded for this project by the Major research and development Projects of Shanxi Province, China (2022ZDYF127), the Basic Research Project of Shanxi Province (202103021224123) and Science and Technology Innovation Fund Project of Shanxi Agricultural University(2018YJ43).

REFERENCES

[1] Collier S., Paschke P., Kay R. R., et al. (2017). Image based modeling of bleb site selection. *Scientific Reports*, Vol.7, pp. 6692, UK.

[2] Gao T., Zhu F., Paul P., et al. (2021). Novel 3D Imaging Systems for High-Throughput Phenotyping of Plants. *Remote Sensing*, Vol. 13, pp. 2113, China.

[3] He J. Q., Harrison R. J., Li B. (2017). A novel 3D imaging system for strawberry phenotyping. *Plant Methods*, Vol. 13, pp. 93 UK.

[4] Lowe D. (2004) Distinctive image features from Scale-Invariant Keypoints. *International Journal of Computer Vision*, Vol. 60, pp. 91-110, UK.

[5] Qi Z., Wang Z., Huang J, et al. (2018) Invalid-point removal based on epipolar constraint in the structured-light method. *Optics and Lasers in Engineering*, Vol. 105, pp.173-181, China.

[6] Qiu Q., Sun N., Bai H., et al. (2019). Field-Based High-Throughput Phenotyping for Maize Plant Using 3D LiDAR Point Cloud Generated With a "Phenomobile". *Frontiers in plant science*, Vol. 10, pp. 554, China.

[7] Rupnik E, Pierrot-Deseilligny M, Delorme A. (2018). 3D reconstruction from multi-view VHR-satellite images in MicMac. *Isprs Journal of Photogrammetry and Remote Sensing*, Vol. 139, pp. 201-211, France.

[8] Schipper, R., van der Meer, M., de Visser, P. H. B., et al. (2023). Consequences of intra-canopy and top LED lighting for uniformity of light distribution in a tomato crop. *Frontiers in plant science*, Vol.14, pp. 1012529, Netherlands.

[9] Seitz S. (2006) A comparison and evaluation of multi-view stereo reconstruction algorithms. *Proceedings of the 2006 IEEE Computer Society Conference on Computer Vision and Pattern Recognition (CVPR'06)*, Vol.1, pp. 519-526, US.

[10] Steve H., Arko L., Jon O. (2015) The Impact of the Calibration Method on the Accuracy of Point Clouds Derived Using Unmanned Aerial Vehicle Multi-View Stereopsis. *Remote Sensing*, Vol.7, pp. 11933-11953, Australia.

[11] Syngelaki M, Hardner M, Oberthuer P, et al. (2018) A new method for non-invasive biomass determination based on stereo photogrammetry. *Bioprocess and Biosystems Engineering*, Vol. 41, pp.369-380, China.

[12] Wen, W., Wang, Y., Wu, S., et al. (2021). 3D phytomer-based geometric modelling method for plants-the case of maize. *Frontiers in Plant Science*, Vol. 13, plab055, China.

[13] Xiang L, Bao Y, Tang L, et al. (2019). Automated morphological traits extraction for sorghum plants via 3D point cloud data analysis. *Computers and Electronics in Agriculture*, Vol. 162, pp. 951-961, China.

[14] Xu B., Yang L. F., Lei B., et al. (2017). A Study of the Accuracy Improvement Strategy for Multi-view 3D Reconstruction Instrument Based on Automatic Calibration Technology. *Acta Geoscientica Sinica*, Vol. 38, pp. 243-248, China.

[15] Zhou F. Q., Cai F. H. (2009), Camera Calibration Method Based on Non-metric Distortion Correction. *Journal of Mechanical Engineering*, Vol.45, pp. 228-232, China.